Am J Physiol Gastrointest Liver Physiol. Author manuscript; available in PMC 2016 July 25.

Published in final edited form as:

Am J Physiol Gastrointest Liver Physiol. 2013 August 15; 305(4): G303–G313. doi:10.1152/ajpgi.00490.2012.

The Na^+/H^+ exchanger isoform 3 is required for active paracellular and transcellular Ca^{2+} transport across murine cecum

Juraj Rievaj[1], **Wanling Pan**[1], **Emmanuelle Cordat**[1], and **R. Todd Alexander**[1,2]

[1]Department of Physiology and Membrane Protein Disease Research Group, University of Alberta, Edmonton, Canada

[2]Department of Pediatrics, University of Alberta, Edmonton, Canada

Abstract

Intestinal calcium (Ca^{2+}) absorption occurs via paracellular and transcellular pathways. Although the transcellular route has been extensively studied, mechanisms mediating paracellular absorption are largely unexplored. Unlike passive diffusion, secondarily active paracellular Ca^{2+} uptake occurs against an electrochemical gradient with water flux providing the driving force. Water movement is dictated by concentration differences that are largely determined by Na^+ fluxes. Consequently, we hypothesized that Na^+ absorption mediates Ca^{2+} flux. NHE3 is central to intestinal Na^+ absorption. NHE3 knockout mice ($NHE3^{-/-}$) display impaired intestinal Na^+, water, and Ca^{2+} absorption. However, the mechanism mediating this latter abnormality is not clear. To investigate this, we used Ussing chambers to measure net Ca^{2+} absorption across different segments of wild-type mouse intestine. The cecum was the only segment with net Ca^{2+} absorption. Quantitative RT-PCR measurements revealed cecal expression of all genes implicated in intestinal Ca^{2+} absorption, including NHE3. We therefore employed this segment for further studies. Inhibition of NHE3 with 100 μM 5-(*N*-ethyl-*N*-isopropyl) amiloride decreased luminal-to-serosal and increased serosal-to-luminal Ca^{2+} flux. $NHE3^{-/-}$ mice had a >60% decrease in luminal-to-serosal Ca^{2+} flux. Ussing chambers experiments under altered voltage clamps (−25, 0, +25 mV) showed decreased transcellular and secondarily active paracellular Ca^{2+} absorption in $NHE3^{-/-}$ mice relative to wild-type animals. Consistent with this, cecal Trpv6 expression was diminished in $NHE3^{-/-}$ mice. Together these results implicate NHE3 in intestinal Ca^{2+} absorption and support the theory that this is, at least partially, due to the role of NHE3 in Na^+ and water absorption.

Address for reprint requests and other correspondence: R. T. Alexander, Dept. of Pediatrics, 4-585 Edmonton Clinic Health Academy, 11405 87th Ave., Univ. of Alberta, Edmonton, Alberta, T6G 2R7, Canada (todd2@ualberta.ca).

DISCLOSURES

No conflicts of interest, financial or otherwise, are declared by the author(s).

AUTHOR CONTRIBUTIONS

J.R., E.C., and R.T.A. conception and design of research; J.R., W.P., and R.T.A. performed experiments; J.R., W.P., and R.T.A. analyzed data; J.R., E.C., and R.T.A. interpreted results of experiments; J.R. and R.T.A. prepared figures; J.R. and R.T.A. drafted manuscript; J.R., W.P., E.C., and R.T.A. edited and revised manuscript; J.R., W.P., E.C., and R.T.A. approved final version of manuscript.

Keywords

NHE3; calcium absorption; cecum

Calcium (Ca^{2+}) homeostasis is central to many physiological processes and is tightly regulated. This is achieved by an orchestrated interplay between the kidneys, bones, and intestine (45). The first step is for Ca^{2+} to be absorbed across the intestine. In humans, all parts of the small intestine participate in Ca^{2+} absorption, with the relative absorption rates generally decreasing from proximal to distal segments (32, 40, 55). The duodenum has the highest relative absorption rate when normalized to unit length of bowel. However, owing to the different lengths of intestinal segments and different sojourn times, the total amount of Ca^{2+} absorbed from more distal parts is likely greater than the amount absorbed from the duodenum (3). Net Ca^{2+} absorption from the colon has also been observed (20).

Transepithelial absorption of Ca^{2+} occurs via two routes, a transcellular and a paracellular pathway. The most widely accepted view of the transcellular pathway is summarized in the facilitated diffusion model. Ca^{2+} ions enter the enterocytes through apical Ca^{2+} channels moving down their electrochemical gradient. Transient receptor potential cation channel subfamily V, member 6 (TRPV6), reportedly performs this function (2). The Ca^{2+} binding protein, calbindin-D_{9K}, facilitates diffusion to the basolateral membrane. Efflux across the basolateral membrane is via the Ca^{2+} pump, PMCA1b, with a minor contribution from the Na^{+}/Ca^{2+} exchanger (21).

Paracellular absorption of Ca^{2+} occurs through the tight junction and intercellular space. The permeability of the tight junction depends on its molecular composition, specifically the expression of claudins (53). Claudin-2, -12, and -15 have been implicated in intestinal paracellular Ca^{2+} flux (8, 18). Both passive and secondarily active paracellular Ca^{2+} flux have been observed (6). The driving force for passive paracellular Ca^{2+} absorption is the concentration difference between lumen and blood, since the potential difference across all intestinal segments is lumen negative. Thus, although significant after the ingestion of food with a high Ca^{2+} content (14), passive paracellular flux of Ca^{2+} may lead to net loss on a Ca^{2+}-poor diet (31, 48).

Secondarily active paracellular flux is the movement of Ca^{2+} ions between epithelial cells, irrespective of the electrochemical gradient. Two mechanisms have been proposed to explain this phenomenon. The first suggests that water removal increases the Ca^{2+} concentration in a thin layer close to the luminal epithelial surface, thereby creating a transepithelial concentration gradient, which in turn provides the driving force for Ca^{2+} absorption (4). The second mechanism, referred to as “solvent drag,” invokes paracellular water flux moving Ca^{2+} by convection (13, 34, 43). The common feature of both mechanisms is a dependence on the absorption of water to induce Ca^{2+} flux.

In the intestine, water movement is osmotically driven by the absorption of monovalent ions, in particular sodium (Na^{+}). Several papers highlight the importance of the sodium/proton exchanger isoform 3 (NHE3) in intestinal water absorption (19, 36, 47). Thus NHE3 is a potential link between transcellular Na^{+} flux and secondarily active paracellular Ca^{2+}

absorption. We have previously explored this possibility (42). The over-expression of NHE3 in opossum kidney cells increased Na^+-dependent transepithelial Ca^{2+} flux. Moreover, NHE3 knockout mice ($NHE3^{-/-}$) displayed impaired Ca^{2+} homeostasis. Intestinal Ca^{2+} uptake measured by gastric gavage was decreased, as was luminal-to-serosal Ca^{2+} flux across the duodenum (42).

However, this work has several limitations. Similar to other studies (7, 8, 52), our Ussing chamber experiments were unidirectional and performed only on duodenal preparations. Furthermore, the gastric gavage experiments measure unidirectional flux across the proximal small intestine. We have been unable to find previous studies that measured the relative contribution of different segments of the intestine to Ca^{2+} absorption in mice. However, previous experiments on rats found that most ingested Ca^{2+} is absorbed from the ileum (12, 37), with the cecum having the highest rate of net Ca^{2+} absorption (16, 26, 38). This creates uncertainty about the physiological significance of measurements made on mouse proximal small intestine.

We therefore measured bidirectional Ca^{2+} fluxes across different intestinal segments in Ussing chambers in the absence of an electrochemical gradient and found net Ca^{2+} absorption in the cecum. We identified mRNA from all genes previously implicated in Ca^{2+} absorption, including NHE3, in both the cecum and the duodenum. Pharmacological inhibition of NHE3 significantly decreased net Ca^{2+} absorption from the cecum. $NHE3^{-/-}$ mice also had decreased net Ca^{2+} flux. To interrogate the mechanism mediating altered Ca^{2+} absorption, we employed a transepithelial voltage-clamp protocol as previously done by others (27). This methodology found that, in $NHE3^{-/-}$ mice, both the transcellular and active paracellular Ca^{2+} absorption pathways are compromised. Our results demonstrate that the cecum is an important player in intestinal Ca^{2+} absorption in mice and highlight the role of NHE3 in this process.

MATERIALS AND METHODS

Ethical approval

All experiments were performed in compliance with the animal ethics board at the University of Alberta, Health Sciences Section, protocol number 576.

Mice

Generation and genotyping of both wild-type and $NHE3^{-/-}$ mice was done as described elsewhere (42). All experiments were performed on wild-type animals unless stated otherwise. Mice were housed in virus-free conditions and maintained on a 12-h light-dark schedule. Standard pelleted chow (PicoLab Rodent Diet 5053; 20% wt/wt protein, 4.5% wt/wt fat, 0.81% wt/wt calcium, 1.07% wt/wt potassium, 0.30% wt/wt sodium, and 2.2 IU/g vitamin D3) and drinking water were available ad libitum. Both male and female animals between 9 and 15 wk of age were used.

Compounds

All chemicals were purchased from Sigma-Aldrich (St. Louis, MO) unless stated otherwise. Amiloride (10 mM stock solution) and tetrodotoxin (TTX) (Alomone Labs, Jerusalem, Israel, 1 mM stock solution) were dissolved in H_2O. Ruthenium red (10 mM stock solution) was dissolved in Ringer's solution. Indomethacin (10 mM stock solution) and forskolin (10 mM stock solution) were dissolved in ethanol, and 5-(*N*-ethyl-*N*-isopropyl) amiloride (EIPA) was dissolved in DMSO. Stock solutions of EIPA and ruthenium red were prepared fresh the day of the experiment. Stock solutions of $^{45}Ca^{2+}$ (PerkinElmer, Billerica, MA), forskolin, and amiloride were stored at +4°C, and stock solutions of TTX (in aliquots) and indomethacin were stored at −20°C.

Ussing chamber experiments

Before starting an experiment, Ringer's solution consisting of 120 mM NaCl, 3 mM KCl, 0.5 mM $MgCl_2$, 1.25 mM $CaCl_2$, 23 mM $NaHCO_3$, 10 mM glucose, and 2 mM mannitol was bubbled thoroughly with 5% vol/vol CO_2, 95% vol/vol O_2. Indomethacin was added (final concentration 2 μM) and the solution was kept ice cold in a sealed container. After euthanasia, specific segments of the mouse intestine were removed by sharp dissection, cut longitudinally along the remnants of the mesenteric attachment, and washed with Ringer's solution. We used intestinal segments between 1 and 4.6 cm distal to the pylorus to represent duodenum. To represent the jejunum, segments between 10 and 14.8 cm distal to the pylorus were used. For ileum, intestine between 3.2 and 6.8 cm proximal to the ileocecal junction was employed. The large intestine was cut perpendicularly to its longitudinal axis at the ileocecal junction. The first 2.4 cm toward the rectum was considered proximal colon; everything left in the opposite direction was considered cecum. The last 2.4 cm of large intestine was considered distal colon. For experiments comparing Ca^{2+} absorption across different parts of the intestine, whole-thickness preparations were initially used. For all subsequent experiments involving cecum and large intestine, the seromusculature was visualized with a dissecting microscope (Olympus SZ60, Olympus America, Center Valley, PA) and gently stripped away with a pair of fine forceps. Cecal area was measured after seromuscular stripping with graph paper. Segments with a length of ≈1.2 cm were mounted in an Ussing chamber (EM-CSYS-2 system with P2400 chambers and P2404 sliders, all from Physiologic Instruments, San Diego, CA). The active surface area for flux studies was 0.25 cm^2. A maximum of four preparations were used from one animal.

Two different protocols were employed to measure Ca^{2+} fluxes across intestinal segments (Fig. 1). After mounting the samples, both parts of the Ussing chambers were filled with 3 (*protocol 1*) or 4 (*protocol 2*) ml of Ringer's solution, maintained at 37°C, and continuously bubbled with 5% vol/vol CO_2-95% vol/vol O_2. The buffering system and recirculation employed minimized the possibility of forming calcium precipitations, which would affect the results. Indomethacin (2 μM bilaterally) and TTX (0.1 μM basolaterally) were used to limit the influence of endogenous prostaglandins and neuronal activity, respectively (11). The transepithelial potential difference was clamped to 0 mV by use of a DVC 1000 amplifier (WPI, Sarasota, FL), and the resulting short-circuit current was recorded through Ag-AgCl electrodes and 3M KCl agarose bridges. The data were collected and stored by use of a PowerLab 8SP series (ADInstruments, Bella Vista, NSW, Australia). The transepithelial

resistance was calculated according to Ohm's law by measuring current changes in response to 2-mV pulses lasting 2.5 s, applied every 100 s. For both protocols, transepithelial resistance and short-circuit current were allowed to stabilize. Then both apical and basolateral solutions were exchanged for fresh ones (both still containing indomethacin and the basolateral solution still containing 0.1 μM TTX), one with $^{45}Ca^{2+}$ added (final activity 5 μCi/ml). Time was set to 0 min and electrical pulses were paused, whereas voltage remained clamped at 0 mV. The chambers were partially covered to limit evaporation. For *protocol 1*, three samples (50 μl each) were taken from both apical and basolateral compartments at 45, 60, 75, and 90 min, which permitted the measurement of unidirectional Ca^{2+} fluxes over three 15-min intervals. For *protocol 2*; four samples (50 μl each) were taken from both the apical and basolateral compartments at 25, 40, 48, 63, 71, 86, 94, and 109 min. After sampling at 40, 63, and 86 min, the voltage clamp was changed alternately to −25 mV, +25 mV, and 0 mV, or +25 mV, −25 mV, and 0 mV, respectively. This allowed the measurement of unidirectional Ca^{2+} fluxes over two 15-min intervals at 0 mV, one 15-min interval at +25 mV, and one 15-min interval at −25 mV for each preparation. We used an 8-min interval in between each of these measurements to allow the tissue to equilibrate at the new voltage. After the last sampling interval, electrical pulses were reinitiated in both protocols to determine possible resistance changes. All measurements with resistance differences greater than 40% were excluded. The reported resistance of each preparation is an average of the resistance measured before and after the experimental period. To further test the viability of the tissue, forskolin was applied bilaterally (final concentration 10 μM) and a short-circuit current increase (peak to basal value) was measured. All preparations included in this study responded with a >50% increase in short-circuit current. For some experiments, preparations from the same animal were paired according to their resistances. A difference in resistance of <25% was required for pairing. For cases where more than two preparations fulfilled this criterion, matching tissues with the least difference in resistance generated pairs.

Sample radioactivity was measured with a LS6500 Multi-Purpose Scintillation Counter (Beckman Coulter, Brea, CA). Ca^{2+} flux was calculated as the rate of $^{45}Ca^{2+}$ appearance in the initially nonradioactive "cold" side (cpm/h) divided by the specific activity of radioactivity in the "hot" side (cpm/mol of Ca^{2+}) as previously described (10). Unless stated otherwise, an average of the fluxes across the three 15-min intervals in *protocol 1* or the two 15-min intervals (first and last one, when the voltage was clamped at 0 mV) in *protocol 2*, was used to calculate the unidirectional Ca^{2+} flux across the preparation. Net Ca^{2+} flux was calculated as the difference between unidirectional Ca^{2+} fluxes in luminal-to-serosal vs. the serosal-to-luminal direction in paired preparations from the same animal. *Protocol 2* was used to calculate the voltage-dependent and voltage-independent contribution to total luminal-to-serosal Ca^{2+} flux as described elsewhere (17). In short, the exponential component of the relationship between the transepithelial voltage and Ca^{2+} flux was first calculated for each potential difference used (i.e., −25, 0 and +25 mV) as $\xi = \exp(z \times F \times PD/R \times T)$, where PD stands for the voltage in which the preparation is clamped, z is the valence of Ca^{2+}, F is Faraday's constant, R is the gas constant, and T is the temperature of the solution. Ca^{2+} flux for each $\xi^{-0.5}$ was then plotted and fit with the linear equation $J_v = J_{vd} \times \xi^{-0.5} + J_{vi}$, where J_v stands for total unidirectional Ca^{2+} flux at a given voltage, J_{vd} is

the voltage-dependent part of J_v under the short-circuit condition, and J_{vi} is the voltage-independent part of J_v. J_{vi} was then calculated for each preparation separately as the *y*-intercept. J_{vd} was calculated as the difference between J_v under the short-circuit condition and J_{vi}. Although serosal-to-luminal flux displayed a variable voltage-independent component, the absolute magnitude of this flux was small. Consequently, for the purpose of this study we assumed the serosal-to-luminal flux across the cecum to be purely passive. Thus, assuming that in the absence of a concentration, electric, or osmotic gradient Ca^{2+} diffusion would be the same in both directions, J_{vd} was further divided into voltage-dependent passive (as determined by serosal-to-luminal flux in a paired preparation) and voltage-dependent active (the difference between J_{vd} and voltage-dependent passive flux) fluxes.

Real-time quantitative PCR

After euthanasia, kidneys and parts of mouse intestine were quickly dissected and snap frozen in liquid nitrogen. Designation of the different intestinal segments used the definitions from above except for cecum, which was additionally divided approximately in half to create a proximal and distal part. This was done as a precaution to avoid accidental overlap with proximal colon. For comparison of gene expression from different intestinal segments, whole thickness intestine was used. For comparison of gene expression between the cecum from wild-type and $NHE3^{-/-}$ mice, the seromusculature was gently removed with fine forceps. Total mRNA was isolated by using TRIzol Reagent (Invitrogen, Carlsbad, CA) according to the manufacturer's instructions. After treatment with DNAseI (AmpGrade; Invitrogen), 1 μg of RNA was reverse transcribed by Random Primers (Invitrogen) and SuperScript II reverse transcriptase (Invitrogen). The cDNA was subsequently used to determine (gene name in parentheses) NHE3 (Slc9a3), calbindin-D_{9K} (S100g), PMCA1b (Atp2b1), NCX1 (Slc8a1), TRPV6 (Trpv6), claudin-2 (cldn2), claudin-12 (cldn12), and claudin-15 (cldn15) mRNA levels. As an internal control mRNA levels of the housekeeping genes actin (actb), GAPDH (gapdh), and the epithelial marker ezrin (ezr) were determined. Expression levels were quantified by PCR (qPCR) on an ABI Prism 7900 HT Sequence Detection System (Applied Biosystems, Foster City, CA). Primers and probes were made by IDT (Integrated DNA Technologies, San Diego, CA) or ABI (Applied Biosystems). The sequences are listed in Table 1.

Statistical analysis

Before analysis, all values were normalized to surface area (cm^2). Data are presented as means ± SE. All data reported are based on measurements made on at least three different animals. Paired or unpaired Student's *t*-tests were carried out to determine statistical significance. Tests were performed using Excel software (Microsoft, Santa Monica, CA), and values <0.05 were considered statistically significant.

RESULTS

The cecum is the only segment of mouse intestine to demonstrate net Ca^{2+} absorption in the absence of an electrochemical gradient

We first measured the net flux of Ca^{2+} across representative segments of the small and large intestine. To do so, whole wall preparations were mounted in Ussing chambers with the same volume of Ringer's solution and identical Ca^{2+} concentrations (1.25 mM) in each hemichamber. The transepithelial voltage was clamped to 0 mV. This experimental design was employed to eliminate the effects of hydrostatic pressure, a Ca^{2+} concentration gradient or electrical potential difference on transepithelial Ca^{2+} movement. Consequently, net transport measured under the given conditions strongly supports active mechanisms mediating Ca^{2+} flux. The cecum was the only part of the mouse intestine where we observed net Ca^{2+} absorption using this methodology (Fig. 2). We found net Ca^{2+} secretion across jejunal segments whereas net transport in the other intestinal segments (including the duodenum) were not significantly different from 0.

As we were unable to detect net Ca^{2+} absorption from mouse duodenum, which has been previously reported (29), we further examined fluxes from this segment. To this end, we separated the duodenum into a proximal (1.0–2.2 cm distally from the pylorus) and distal portion (3.4–4.6 cm distally from the pylorus) and performed analysis on these different portions separately (Table 2). Given the length of the different portions, calculation of net Ca^{2+} absorption was not possible, since it would require "pairing" between samples from different animals. However, we were unable to detect a significant difference in unilateral fluxes in either direction between proximal and distal parts of the duodenum. Furthermore, we attempted to increase the sensitivity of our assay by performing seromuscular stripping on samples from the large intestine. This resulted in a nonsignificant increase in net Ca^{2+} absorption relative to whole-thickness preparations in all segments studied (i.e., cecum, proximal colon, and distal colon). In contrast to the cecum, net Ca^{2+} fluxes from proximal and distal colon, after seromuscular stripping, were not significantly different from 0 (although there was a tendency toward net absorption). Taken together, these results imply an important role for the cecum in intestinal Ca^{2+} absorption in mice, as has been reported for rats (9, 24, 26, 38).

The cecum expresses all genes implicated in intestinal Ca^{2+} absorption, including NHE3

We next examined the expression of mRNA from genes known to be associated with transcellular and paracellular Ca^{2+} transport. Whole wall preparations (from both male and female mice) identical to that used in the Ussing chamber studies were used for mRNA isolation and kidney samples were included as a control. We normalized expression to the epithelial marker ezrin (Fig. 3, *A*–*H*), although comparable results were obtained when GAPDH was used for normalization since both ezrin and GAPDH showed a similar expression profile (Fig. 3, *I* and *J*). Significant Trpv6 expression was found in duodenum, cecum, and distal colon. However, Trpv6 expression was very low in ileum and proximal colon and undetectable in jejunum (Fig. 3*A*). Similarly, calbindin-D_{9K} was expressed in duodenum, cecum, and proximal colon whereas expression was very low in jejunum, ileum, and distal colon (Fig. 3*B*). NCX1 and PMCa1b were expressed across all intestinal

segments. NCX1 expression was much higher throughout the entire colon than in duodenum whereas PMCa1b levels were higher in duodenum than in more distal parts of the intestine (Fig. 3, *C* and *D*). Expression levels of claudin-2 and −12 were similar throughout the intestine. Claudin-15 expression was higher in the duodenum than in more distal intestinal segments (Fig. 3, *E*–*G*). NHE3 was expressed throughout the intestine (Fig. 3*H*). The expression of Trpv5 and calbindin-D_{28k} was, compared with the kidney, very low or undetectable across all intestinal segments (data not shown). These results confirm that the cecum expresses all genes previously implicated in Ca^{2+} absorption from the intestine, including NHE3.

Pharmacological inhibition of NHE3 decreases luminal-to-serosal Ca^{2+} flux and increases serosal-to-luminal Ca^{2+} flux across mouse cecum

The cecum was the only part of the intestine to demonstrate net Ca^{2+} absorption and it expressed NHE3. We therefore used this segment to explore the mechanism by which NHE3 alters intestinal Ca^{2+} absorption. All of the following experiments were performed on cecal preparations after seromuscular stripping. *Protocol 1* (Fig. 1) was first employed to determine the effect of pharmacological inhibition of NHE3 activity on transepithelial Ca^{2+} movement. Fluxes from three subsequent time periods were measured and the fluxes from the first and third periods were compared. In the absence of drugs, the difference in flux between the first and the third interval was less than 7% in the luminal-to-serosal direction and less than 3% in the serosal-to-luminal direction. Neither difference was statistically significant (Fig. 4, *A* and *B*). These results support the use of *protocol 1* to test the effect of pharmacological inhibitors on Ca^{2+} flux when a drug is added in the beginning of the second time period. To separate NHE3 activity from NHE2 and ENaC activities, we pretreated preparations with amiloride (10 μM, apically at the beginning of the 45-min incubation period). This blocks NHE2 and ENaC activity while leaving NHE3 activity largely unaltered (5, 50, 51). In the presence of amiloride, there was still no difference in Ca^{2+} flux between the first and third time period (data not shown). NHE3 activity was then blocked by the addition of EIPA (100 μM, bilaterally) after the first time period (50). This permitted the comparison of Ca^{2+} fluxes in the presence and absence of NHE3 activity across each preparation. After inhibition of NHE3, luminal-to-serosal Ca^{2+} flux was significantly reduced by nearly 30% (Student's paired *t*-test, $P < 0.01$), whereas flux in the opposite direction was significantly increased by 23% (Student's paired *t*-test, $P < 0.05$) (Fig. 4, *C* and *D*). There was no effect of amiloride addition on Ca^{2+} flux in either direction when values from the first intervals were compared with and without amiloride pretreatment (Student's unpaired *t*-test, $P > 0.95$) (Fig. 4, *E* and *F*). These data demonstrate that NHE3 participates in Ca^{2+} absorption across mouse cecum.

Ruthenium red, an inhibitor of TRPV6, blocks voltage-independent Ca^{2+} flux

To distinguish between paracellular and transcellular Ca^{2+} flux across mouse cecum we utilized a modified voltage-clamp protocol (*protocol 2* in Fig. 1) previously used by others to this end (17, 31, 39). We were concerned that altering the potential difference across the apical membrane with this protocol might affect the activity of apically localized Ca^{2+} channels such as TRPV6, thus altering both transcellular and paracellular Ca^{2+} fluxes (22). Therefore we first tested the effect of a TRPV6 inhibitor before using this method to

investigate the role of NHE3 in intestinal Ca^{2+} absorption. Preparations from the same animal were paired according to their resistance, and *protocol 2* was applied to them simultaneously. One preparation from each pair was pretreated with ruthenium red, a TRPV6 blocker (50 μM apically at the beginning of the 25-min incubation period). Fluxes were measured in the luminal-to-serosal direction and the contribution of voltage-dependent and voltage-independent Ca^{2+} flux was determined. Voltage-independent flux [assumed to represent the transcellular absorption pathway (27)] was responsible for ~60% of Ca^{2+} flux across preparations without ruthenium red pretreatment, the remaining flux was voltage dependent (assumed to represent paracellular flux). Apically applied ruthenium red blocked more than 40% of the voltage-independent flux without altering voltage-dependent flux (Fig. 5). The observed effect was side specific since there was no inhibition in Ca^{2+} flux when ruthenium red was added basolaterally (data not shown). These results confirm that the voltage-clamp protocol can distinguish between paracellular (voltage-dependent) and transcellular (voltage-independent) Ca^{2+} absorption.

NHE3$^{-/-}$ mice have decreased voltage-independent and active voltage-dependent Ca^{2+} absorption

We initially intended to use the voltage-clamp protocol to distinguish between the voltage-dependent and voltage-independent effects of EIPA on Ca^{2+} flux. However, prolonged exposure to EIPA and/or amiloride during *protocol 2*, which occurs over a much longer period of time relative to *protocol 1*, led to a large decrease in transepithelial resistance accompanied by large increases in Ca^{2+} flux during the second 0-mV period (relative to the first one; data not shown). Therefore, we used NHE3$^{-/-}$ mice to further interrogate the role of NHE3 in cecal Ca^{2+} absorption. The properties of cecal preparations from NHE3$^{-/-}$ mice are summarized in Table 3. As previously reported (47), NHE3$^{-/-}$ mice have enlargement of all parts of their intestine compared with wild-type mice. We confirmed this observation by measuring the total area of cecum (after seromuscular stripping), which was on average 2.5 times larger in the knockout animals. The average transepithelial resistance was significantly increased across the cecum of knockout animals (Student's unpaired *t*-test, $P < 0.05$). The average short-circuit current was also increased (Student's unpaired *t*-test, $P < 0.05$) similar to what was previously shown for distal colon (47).

Previously, paired preparations from the same animal were used to investigate the effect of drugs on Ca^{2+} transport. This approach cannot be used to compare between wild-type and NHE3$^{-/-}$ mice. Because of the fact that we cannot exclude an effect of sex or age on Ca^{2+} movement across our preparations, we first compared the fluxes between wild-type animals of both sexes. There was no difference in luminal-to-serosal, serosal-to-luminal, or net Ca^{2+} fluxes between males and females of similar age (Table 4). The calculated contribution of voltage-independent and active voltage-dependent flux to total luminal-to-serosal flux was also not different between sexes (Student's unpaired *t*-test, $P > 0.05$) (Table 4). Thus data from both sexes were pooled for the comparison of Ca^{2+} fluxes between wild-type (5 males and 5 females, 10.8 ± 0.6 wk old) and NHE3 knockout (2 males and 3 females, 10.9 ± 1.4 wk old) mice. The age of mice was not significantly different between groups (Student's unpaired *t*-test, $P > 0.05$).

Compared with wild-type animals, the net Ca^{2+} absorption across the cecum of $NHE3^{-/-}$ mice was significantly reduced by 78% (Student's unpaired *t*-test, $P < 0.01$). This was predominantly due to a >60% decrease of Ca^{2+} flux in the luminal-to-serosal direction (Student's unpaired *t*-test, $P < 0.01$) since flux in the opposite direction was not significantly altered (Fig. 6*A*). When comparing luminal-to-serosal fluxes, we observed a significant decrease in the voltage-independent portion of flux in $NHE3^{-/-}$ mice (81% decrease, Student's unpaired *t*-test, $P < 0.01$). Voltage-dependent flux was divided into an active and passive component as described in MATERIALS AND METHODS: the passive component was assumed to equal the total flux in the serosal-to-luminal direction and the remaining flux was designated the active paracellular component. The active voltage-dependent (i.e., active paracellular) portion of Ca^{2+} absorption (which contributed ≈20% to the total unilateral flux in wild-type animals) was significantly decreased by ≈70% (Student's unpaired *t*-test, $P < 0.05$) whereas the passive voltage-dependent portion was not significantly altered in $NHE3^{-/-}$ mice (Fig. 6*B*). These results demonstrate that, in $NHE3^{-/-}$ mice, both voltage-independent and active voltage-dependent pathways of Ca^{2+} absorption are impaired.

$NHE3^{-/-}$ mice have diminished cecal Trpv6 mRNA expression

The above results suggest that decreased Ca^{2+} absorption across the cecum of $NHE3^{-/-}$ mice was at least partly due to decreased transcellular Ca^{2+} absorption. We therefore examined the expression of genes relevant to this pathway by qPCR. We used cecum after seromuscular stripping as the source of mRNA to facilitate comparison of the results with the functional data. Trpv6 expression was dramatically reduced in the knockout animals (98% decrease, Student's unpaired *t*-test, $P < 0.05$). NCX1 expression was decreased by 28% although this did not reach statistical significance (Student's unpaired *t*-test, $P = 0.062$, Fig. 7). Calbindin-D_{9K} and PMCa1b expression were not different between wild-type and knockout animals. We normalized expression to the epithelial marker ezrin; however, comparable results were obtained when GAPDH or β-actin was used (with the exception of a reduction in NCX1 expression in $NHE3^{-/-}$ mice, which reached statistical significance when normalized to β-actin, data not shown). These results raise the possibility that decreased apical influx through TRPV6 is responsible for impaired transcellular Ca^{2+} absorption from the cecum of $NHE3^{-/-}$ mice.

DISCUSSION

We measured bidirectional Ca^{2+} fluxes across preparations from different segments of mouse intestine. The cecum was the only segment to demonstrate net Ca^{2+} absorption. The cecum expresses NHE3 as well as all genes implicated in intestinal Ca^{2+} absorption. Consequently, we used this segment to investigate the role of NHE3 in transepithelial Ca^{2+} flux. Pharmacological inhibition of NHE3 decreased luminal-to-serosal flux and increased serosal-to-luminal flux, suggesting that NHE3 contributes to active paracellular Ca^{2+} absorption. After demonstrating that the voltage-clamp protocol can distinguish between paracellular and transcellular Ca^{2+} absorption, we found that $NHE3^{-/-}$ mice had decreased total, transcellular, and active paracellular Ca^{2+} absorption. Impairment in transcellular Ca^{2+} absorption was potentially mediated by decreased Trpv6 expression in $NHE3^{-/-}$ mice.

In the absence of an electrochemical gradient, the cecum was the only intestinal segment with net Ca^{2+} absorption, whereas net Ca^{2+} secretion was found across the jejunum. Although we are unaware of comparable work performed on mice, our data are consistent with similar experiments performed on rats (16, 26). The most striking difference is the absence of net Ca^{2+} absorption from mouse duodenum. Differences between species or differences in experimental protocols may account for this. In the absence of an electrochemical gradient across rat duodenum, the direction of net Ca^{2+} flux depends on the Ca^{2+} concentration of the solutions bathing the tissue. When both luminal and serosal Ca^{2+} is >1.25 mM (54) or >2.5 mM (25) net secretion is observed; however, below these values net absorption is reported. This is because Ca^{2+} secretion is a nonsaturable process, whereas Ca^{2+} absorption contains both a saturable and a nonsaturable component (25). We used a Ca^{2+} concentration of 1.25 mM, roughly equal to the concentration of free Ca^{2+} in blood. We suspect that the use of a lower Ca^{2+} concentration [perhaps with magnesium removal (28)] would “uncover” net Ca^{2+} absorption across the duodenum. We elected not to perform this experiment since its physiological significance is questionable. Since the first centimeter of duodenum was not used in the present study, the possibility remains that net duodenal Ca^{2+} absorption occurs exclusively there. Consistent with this, the expression of genes implicated in transcellular calcium flux decreases much more rapidly with distance from the pylorus in mice relative to rats (23). We were unable to test this experimentally as at least two paired segments (each ~1.2 cm long) from the same animal are required to determine net Ca^{2+} flux. It is questionable whether active Ca^{2+} absorption from such a restricted area, given the rapid passage of luminal contents would be physiologically significant.

Our functional data are supported by the qPCR results. The cecum expresses all genes implicated in transcellular and paracellular Ca^{2+} absorption, including NHE3. This is in agreement with results obtained from rats (30). We employed intestine without seromuscular stripping in our qPCR experiments. Therefore we cannot conclude that the genes studied are expressed in the intestinal epithelium and not in subepithelial cells such as smooth muscle, neurons, endothelium, or peritoneum. However, as seen in Fig. 7, stripping of the seromuscular layer from cecal preparations did not prevent the detection of genes implicated in transcellular Ca^{2+} absorption, increasing the probability that our qPCR data are relevant to intestinal Ca^{2+} transport. As a housekeeping gene, we used ezrin, which showed a similar expression profile to GAPDH. As apparent from Fig. 3, *I* and *J*, both genes had somewhat higher expression in the large intestine relative to the small intestine. Thus normalization to either gene underestimates the relative expression of genes of interest in the large intestine.

The importance of the cecum in rat intestinal Ca^{2+} absorption and Ca^{2+} homeostasis in general has recently been demonstrated (9, 24, 26, 38). Consistent with a role for NHE3 in cecal Ca^{2+} absorption, this process is partly dependent on luminal Na^+ and basolateral Na^+-K^+-ATPase activity (16). Net water and Na^+ absorption from rat cecum, as well as the interdependency of the former on the later, has been demonstrated, with Na^+ absorption occurring in an electroneutral fashion and displaying pharmacological sensitivity typical of NHE3 (15, 35, 46). Intestinal water absorption is impaired in $NHE3^{-/-}$ mice with the greatest intraluminal water retention occurring in the cecum (47). Significant NHE3 mRNA expression has been observed in mouse cecum previously (47) although two studies have failed to detect NHE3 protein in this part of the large intestine (41, 49), perhaps because of

the antibody employed. We observed significant NHE3 mRNA expression in both the proximal and distal halves of mouse cecum, ruling out the possibility of border overlap with proximal colon. There is therefore an abundance of evidence supporting the presence of functional NHE3 in the cecum of rodents and its contribution to water reabsorption. Consequently, the cecum is the ideal site to explore how NHE3 contributes to intestinal Ca^{2+} absorption in mice.

We found that pharmacological inhibition of NHE3 with EIPA decreased luminal-to-serosal Ca^{2+} flux by nearly 30%, supporting a connection between Na^{+} and Ca^{2+} absorption. The significant increase of Ca^{2+} flux in the opposite direction strongly implies that NHE3 participates in active paracellular Ca^{2+} flux. If the effect of EIPA was to block the transcellular pathway, increased backflux should not have been observed. Moreover, if EIPA caused a decrease in passive paracellular flux, because of a decrease in paracellular permeability for example, this effect would likely have been bidirectional and we would have observed a decrease in Ca^{2+} flux in the serosal-to-luminal direction. In contrast, reduced water absorption, as would occur in the absence of NHE3 activity, would decrease the “secondary concentration gradient” between thin unstirred layers of liquid close to the epithelial surface and/or decrease the amount of water flow through the intercellular space, thus increasing the speed of Ca^{2+} flow in the opposite direction in either model of active paracellular flux.

To measure the relative contribution of paracellular and transcellular Ca^{2+} absorption across mouse cecum, we used a voltage-clamp method previously used on rat cecum (26, 38). It is based on the assumption that a transepithelial potential difference will affect ion movement exclusively through the paracellular pathway (voltage-dependent flow). This might not necessarily be the case. An applied voltage will alter the transmembrane potential across both the apical and basolateral membranes. Voltage changes across the basolateral membrane should not greatly affect Ca^{2+} flux because of the nature of the transporters mediating Ca^{2+} efflux there. However, Ca^{2+} in-flux across the apical membrane occurs through ion channel(s) and therefore is voltage sensitive. TRPV6, a voltage-gated Ca^{2+} channel, has been proposed to fulfill this function. We therefore sought to test the assumption that voltage-independent flux represents the transcellular pathway by using the TRPV6 blocker ruthenium red. Consistent with our assumptions, ruthenium red did not alter voltage-dependent Ca^{2+} flux (i.e., paracellular) and significantly decreased voltage-independent flux (i.e., transcellular).

Ruthenium red did not completely block voltage-independent Ca^{2+} flux. One explanation for this is that TRPV6 might not be the only Ca^{2+} influx pathway across the apical membrane. This explanation is supported by results from Ca^{2+} flux studies across the intestine of Trpv6 knockout animals, which showed only a partial reduction in intestinal Ca^{2+} absorption (1, 2, 33). Alternatively, part of the voltage-independent flux may occur via the paracellular pathway, leading to an underestimation of paracellular flow by this method. Regardless, our data support the rationale for using a voltage-clamp protocol to distinguish between paracellular and transcellular Ca^{2+} absorption pathways.

With this methodology, ≈60% of total Ca^{2+} flux across mouse cecum occurred in a voltage-independent or transcellular manner, slightly more than what has been observed in rats (26). We further divided the voltage-dependent fraction into a passive (i.e., paracellular diffusion) and active component. The voltage-dependent passive component was assumed to be equal in both directions, as expected for diffusional flow. As discussed in MATERIALS AND METHODS, we considered all serosal-to-luminal flow to be diffusional and paracellular. On the basis of these assumptions, 23% of net Ca^{2+} flux across mouse cecum was determined to occur via an active paracellular process. Because of the abovementioned reasons, this is likely an underestimate.

$NHE3^{-/-}$ mice had dramatically reduced net Ca^{2+} flux, further confirming a role for NHE3 in Ca^{2+} absorption. Decreased Ca^{2+} absorption was due to a significant decrease in both transcellular and active paracellular Ca^{2+} flux. Despite the increase in transepithelial resistance, passive paracellular transport was not significantly different from that of wild-type mice. Decreased voltage-independent or transcellular Ca^{2+} flux in our experiments is consistent with the decreased Trpv6 expression observed in $NHE3^{-/-}$ mice. The decrease in transcellular Ca^{2+} flux was much larger than observed when employing ruthenium red in wild-type animals, implying an additional downregulation of another transcellular pathway in $NHE3^{-/-}$ mice.

We can only speculate about the mechanism mediating decreased cecal Trpv6 expression in $NHE3^{-/-}$ mice, animals known to have increased $1,25(OH)_2D_3$ levels (42). Vitamin D attenuates the effects of the renin-angiotensin system (RAS) (44). $NHE3^{-/-}$ mice are volume depleted and have dramatically elevated renin and aldosterone levels. Perhaps the RAS attenuates vitamin D signaling, leading to decreased Trpv6 expression in $NHE3^{-/-}$ mice. Trpv6 expression was significantly reduced in the cecum but not the duodenum (42) perhaps because cecal Ca^{2+} absorption is more sensitive to hormonal regulation than similar process in the duodenum. Both these possibilities remain to be proven experimentally.

In conclusion, we found that, when investigated in Ussing chambers, the cecum is the site of greatest Ca^{2+} absorption in mice. Furthermore, using both genetic and pharmacological approaches we have implicated NHE3 in cecal Ca^{2+} absorption. Our data support the theory that this is at least partially due to the role of NHE3 in Na^+ and water absorption, although we cannot exclude the involvement of NHE3 in transcellular Ca^{2+} absorption. Thus NHE3 provides a molecular link between Na^+, water, and Ca^{2+} absorptive processes in the intestine.

Acknowledgments

GRANTS

This work was funded by a grant from the Canadian Institute of Health Research (CIHR). R. T. Alexander is supported by a Clinician Scientist Award from CIHR and an Alberta Innovates Health Solutions Clinical Investigator Award. E. Cordat is a KRESCENT New Investigator.

References

1. Benn BS, Ajibade D, Porta A, Dhawan P, Hediger M, Peng JB, Jiang Y, Oh GT, Jeung EB, Lieben L, Bouillon R, Carmeliet G, Christakos S. Active intestinal calcium transport in the absence of transient receptor potential vanilloid type 6 and calbindin-D_{9k}. Endocrinology. 2008; 149:3196–3205. [PubMed: 18325990]
2. Bianco SD, Peng JB, Takanaga H, Suzuki Y, Crescenzi A, Kos CH, Zhuang L, Freeman MR, Gouveia CH, Wu J, Luo H, Mauro T, Brown EM, Hediger MA. Marked disturbance of calcium homeostasis in mice with targeted disruption of the Trpv6 calcium channel gene. J Bone Miner Res. 2007; 22:274–285. [PubMed: 17129178]
3. Birge SJ, Peck WA, Berman M, Whedon GD. Study of calcium absorption in man: a kinetic analysis and physiologic model. J Clin Invest. 1969; 48:1705–1713. [PubMed: 5822579]
4. Bomsztyk K, Wright FS. Dependence of ion fluxes on fluid transport by rat proximal tubule. Am J Physiol Renal Fluid Electrolyte Physiol. 1986; 250:F680–F689.
5. Canessa CM, Schild L, Buell G, Thorens B, Gautschi I, Horisberger JD, Rossier BC. Amiloride-sensitive epithelial Na^+ channel is made of three homologous subunits. Nature. 1994; 367:463–467. [PubMed: 8107805]
6. Charoenphandhu N, Krishnamra N. Prolactin is an important regulator of intestinal calcium transport. Can J Physiol Pharmacol. 2007; 85:569–581. [PubMed: 17823618]
7. Charoenphandhu N, Limlomwongse L, Krishnamra N. Prolactin directly enhanced Na^+/K^+- and Ca^{2+}-ATPase activities in the duodenum of female rats. Can J Physiol Pharmacol. 2006; 84:555–563. [PubMed: 16902601]
8. Charoenphandhu N, Nakkrasae LI, Kraidith K, Teerapornpuntakit J, Thongchote K, Thongon N, Krishnamra N. Two-step stimulation of intestinal Ca^{2+} absorption during lactation by long-term prolactin exposure and suckling-induced prolactin surge. Am J Physiol Endocrinol Metab. 2009; 297:E609–E619. [PubMed: 19567804]
9. Charoenphandhu N, Suntornsaratoon P, Jongwattanapisan P, Wongdee K, Krishnamra N. Enhanced trabecular bone resorption and microstructural bone changes in rats after removal of the cecum. Am J Physiol Endocrinol Metab. 2012; 303:E1069–E1075. [PubMed: 22912366]
10. Charoenphandhu N, Tudpor K, Pulsook N, Krishnamra N. Chronic metabolic acidosis stimulated transcellular and solvent drag-induced calcium transport in the duodenum of female rats. Am J Physiol Gastrointest Liver Physiol. 2006; 291:G446–G455. [PubMed: 16675746]
11. Clarke LL. A guide to Ussing chamber studies of mouse intestine. Am J Physiol Gastrointest Liver Physiol. 2009; 296:G1151–G1166. [PubMed: 19342508]
12. Cramer CF, Copp DH. Progress and rate of absorption of radiostrontium through intestinal tracts of rats. Proc Soc Exp Biol Med. 1959; 102:514–517. [PubMed: 13812617]
13. Diamond JM, Bossert WH. Standing-gradient osmotic flow. A mechanism for coupling of water and solute transport in epithelia. J Gen Physiol. 1967; 50:2061–2083. [PubMed: 6066064]
14. Duflos C, Bellaton C, Pansu D, Bronner F. Calcium solubility, intestinal sojourn time and paracellular permeability codetermine passive calcium absorption in rats. J Nutr. 1995; 125:2348–2355. [PubMed: 7666252]
15. Escobar E, Ibarra C, Todisco E, Parisi M. Water and ion handling in the rat cecum. Am J Physiol Gastrointest Liver Physiol. 1990; 259:G786–G791.
16. Favus MJ. Factors that influence absorption and secretion of calcium in the small intestine and colon. Am J Physiol Gastrointest Liver Physiol. 1985; 248:G147–G157.
17. Frizzell RA, Schultz SG. Ionic conductances of extracellular shunt pathway in rabbit ileum. Influence of shunt on transmural sodium transport and electrical potential differences. J Gen Physiol. 1972; 59:318–346. [PubMed: 5058963]
18. Fujita H, Sugimoto K, Inatomi S, Maeda T, Osanai M, Uchiyama Y, Yamamoto Y, Wada T, Kojima T, Yokozaki H, Yamashita T, Kato S, Sawada N, Chiba H. Tight junction proteins claudin-2 and -12 are critical for vitamin D-dependent Ca^{2+} absorption between enterocytes. Mol Biol Cell. 2008; 19:1912–1921. [PubMed: 18287530]

19. Gawenis LR, Stien X, Shull GE, Schultheis PJ, Woo AL, Walker NM, Clarke LL. Intestinal NaCl transport in NHE2 and NHE3 knockout mice. Am J Physiol Gastrointest Liver Physiol. 2002; 282:G776–G784. [PubMed: 11960774]
20. Grinstead WC, Pak CY, Krejs GJ. Effect of 1,25-dihydroxyvitamin D_3 on calcium absorption in the colon of healthy humans. Am J Physiol Gastrointest Liver Physiol. 1984; 247:G189–G192.
21. Hoenderop JG, Nilius B, Bindels RJ. Calcium absorption across epithelia. Physiol Rev. 2005; 85:373–422. [PubMed: 15618484]
22. Hoenderop JG, Vennekens R, Muller D, Prenen J, Droogmans G, Bindels RJ, Nilius B. Function and expression of the epithelial Ca^{2+} channel family: comparison of mammalian ECaC1 and 2. J Physiol. 2001; 537:747–761. [PubMed: 11744752]
23. Huybers S, Naber TH, Bindels RJ, Hoenderop JG. Prednisolone-induced Ca^{2+} malabsorption is caused by diminished expression of the epithelial Ca^{2+} channel T.RPV6. Am J Physiol Gastrointest Liver Physiol. 2007; 292:G92–G97. [PubMed: 16901990]
24. Jongwattanapisan P, Suntornsaratoon P, Wongdee K, Dorkkam N, Krishnamra N, Charoenphandhu N. Impaired body calcium metabolism with low bone density and compensatory colonic calcium absorption in cecectomized rats. Am J Physiol Endocrinol Metab. 2012; 302:E852–E863. [PubMed: 22275757]
25. Karbach U. Segmental heterogeneity of cellular and paracellular calcium transport across the rat duodenum and jejunum. Gastroenterology. 1991; 100:47–58. [PubMed: 1898496]
26. Karbach U, Feldmeier H. The cecum is the site with the highest calcium absorption in rat intestine. Dig Dis Sci. 1993; 38:1815–1824. [PubMed: 8404402]
27. Karbach U, Rummel W. Cellular and paracellular calcium transport in the rat ileum and the influence of 1 alpha, 25-dihydroxyvitamin D_3 and dexamethasone. Naunyn Schmiedebergs Arch Pharmacol. 1987; 336:117–124. [PubMed: 3114650]
28. Karbach U, Schmitt A, Saner FH. Different mechanism of magnesium and calcium transport across rat duodenum. Dig Dis Sci. 1991; 36:1611–1618. [PubMed: 1935500]
29. Khuituan P, Teerapornpuntakit J, Wongdee K, Suntornsaratoon P, Konthapakdee N, Sangsaksri J, Sripong C, Krishnamra N, Charoenphandhu N. Fibroblast growth factor-23 abolishes 1,25-dihydroxyvitamin D_3-enhanced duodenal calcium transport in male mice. Am J Physiol Endocrinol Metab. 2012; 302:E903–E913. [PubMed: 22275752]
30. Kraidith K, Jantarajit W, Teerapornpuntakit J, Nakkrasae LI, Krishnamra N, Charoenphandhu N. Direct stimulation of the transcellular and paracellular calcium transport in the rat cecum by prolactin. Pflügers Arch. 2009; 458:993–1005. [PubMed: 19449156]
31. Krawitt EL, Schedl HP. In vivo calcium transport by rat small intestine. Am J Physiol. 1968; 214:232–236. [PubMed: 5635865]
32. Krejs GJ, Nicar MJ, Zerwekh JE, Norman DA, Kane MG, Pak CY. Effect of 1,25-dihydroxyvitamin D_3 on calcium and magnesium absorption in the healthy human jejunum and ileum. Am J Med. 1983; 75:973–976. [PubMed: 6689108]
33. Kutuzova GD, Sundersingh F, Vaughan J, Tadi BP, Ansay SE, Christakos S, Deluca HF. TRPV6 is not required for 1alpha, 25- dihydroxyvitamin D_3-induced intestinal calcium absorption in vivo. Proc Natl Acad Sci USA. 2008; 105:19655–19659. [PubMed: 19073913]
34. Larsen EH, Nedergaard S, Ussing HH. Role of lateral intercellular space and sodium recirculation for isotonic transport in leaky epithelia. Rev Physiol Biochem Pharmacol. 2000; 141:153–212. [PubMed: 10916425]
35. Loeschke K, Gordon HA. Water movement across the cecal wall of the germfree rat. Proc Soc Exp Biol Med. 1970; 133:1217–1222. [PubMed: 5440409]
36. Maher MM, Gontarek JD, Bess RS, Donowitz M, Yeo CJ. The Na^+/H^+ exchange isoform NHE3 regulates basal canine ileal Na^+ absorption in vivo. Gastroenterology. 1997; 112:174–183. [PubMed: 8978356]
37. Marcus CS, Lengemann FW. Absorption of Ca^{45} and Sr^{85} from solid and liquid food at various levels of the alimentary tract of the rat. J Nutr. 1962; 77:155–160. [PubMed: 14469699]
38. Nellans HN, Goldsmith RS. Transepithelial calcium transport by rat cecum: high-efficiency absorptive site. Am J Physiol Gastrointest Liver Physiol. 1981; 240:G424–G431.

39. Nellans HN, Kimberg DV. Cellular and paracellular calcium transport in rat ileum: effects of dietary calcium. Am J Physiol Endocrinol Metab Gastrointest Physiol. 1978; 235:E726–E737.
40. Norman DA, Fordtran JS, Brinkley LJ, Zerwekh JE, Nicar MJ, Strowig SM, Pak CY. Jejunal and ileal adaptation to alterations in dietary calcium: changes in calcium and magnesium absorption and pathogenetic role of parathyroid hormone and 1,25-dihydroxyvitamin D. J Clin Invest. 1981; 67:1599–1603. [PubMed: 7240409]
41. Okamoto K, Hanazaki K, Akimori T, Okabayashi T, Okada T, Kobayashi M, Ogata T. Immunohistochemical and electron microscopic characterization of brush cells of the rat cecum. Med Mol Morphol. 2008; 41:145–150. [PubMed: 18807140]
42. Pan W, Borovac J, Spicer Z, Hoenderop JG, Bindels RJ, Shull GE, Doschak MR, Cordat E, Alexander RT. The epithelial sodium/proton exchanger, NHE3, is necessary for renal and intestinal calcium (re)absorption. Am J Physiol Renal Physiol. 2012; 302:F943–F956. [PubMed: 21937605]
43. Pappenheimer JR, Reiss KZ. Contribution of solvent drag through intercellular junctions to absorption of nutrients by the small intestine of the rat. J Membr Biol. 1987; 100:123–136. [PubMed: 3430569]
44. Porsti IH. Expanding targets of vitamin D receptor activation: downregulation of several RAS components in the kidney. Kidney Int. 2008; 74:1371–1373. [PubMed: 19008907]
45. Renkema KY, Alexander RT, Bindels RJ, Hoenderop JG. Calcium and phosphate homeostasis: concerted interplay of new regulators. Ann Med. 2008; 40:82–91. [PubMed: 18293139]
46. Schreiner J, Weber M, Loeschke K. Sodium chloride transport of normal and dietary enlarged rat cecum in vitro. Digestion. 1998; 59:676–682. [PubMed: 9813393]
47. Schultheis PJ, Clarke LL, Meneton P, Miller ML, Soleimani M, Gawenis LR, Riddle TM, Duffy JJ, Doetschman T, Wang T, Giebisch G, Aronson PS, Lorenz JN, Shull GE. Renal and intestinal absorptive defects in mice lacking the NHE3 Na^+/H^+ exchanger. Nat Genet. 1998; 19:282–285. [PubMed: 9662405]
48. Sernka TJ, Borle AB. Calcium in the intestinal contents of rats on different calcium diets. Proc Soc Exp Biol Med. 1969; 131:1420–1423. [PubMed: 5812009]
49. Talbot C, Lytle C. Segregation of Na/H exchanger-3 and Cl/HCO_3 exchanger SLC26A3 (DRA) in rodent cecum and colon. Am J Physiol Gastrointest Liver Physiol. 2010; 299:G358–G367. [PubMed: 20466943]
50. Tse CM, Levine SA, Yun CH, Brant SR, Pouyssegur J, Montrose MH, Donowitz M. Functional characteristics of a cloned epithelial Na^+/H^+ exchanger (NHE3): resistance to amiloride and inhibition by protein kinase C. Proc Natl Acad Sci USA. 1993; 90:9110–9114. [PubMed: 8415663]
51. Tse CM, Levine SA, Yun CH, Montrose MH, Little PJ, Pouyssegur J, Donowitz M. Cloning and expression of a rabbit cDNA encoding a serum-activated ethylisopropylamiloride-resistant epithelial Na^+/H^+ exchanger isoform (NHE-2). J Biol Chem. 1993; 268:11917–11924. [PubMed: 7685025]
52. Tudpor K, Teerapornpuntakit J, Jantarajit W, Krishnamra N, Charoenphandhu N. 1,25-Dihydroxyvitamin D_3 rapidly stimulates the solvent drag-induced paracellular calcium transport in the duodenum of female rats. J Physiol Sci. 2008; 58:297–307. [PubMed: 18838052]
53. Van Itallie CM, Anderson JM. Claudins and epithelial paracellular transport. Annu Rev Physiol. 2006; 68:403–429. [PubMed: 16460278]
54. Walling MW, Kimberg DV. Active secretion of calcium, sodium and chloride by adult rat duodenum in vitro. Biochim Biophys Acta. 1975; 382:213–217. [PubMed: 1120156]
55. Wensel RH, Rich C, Brown AC, Volwiler W. Absorption of calcium measured by intubation and perfusion of the intact human small intestine. J Clin Invest. 1969; 48:1768–1775. [PubMed: 5822585]

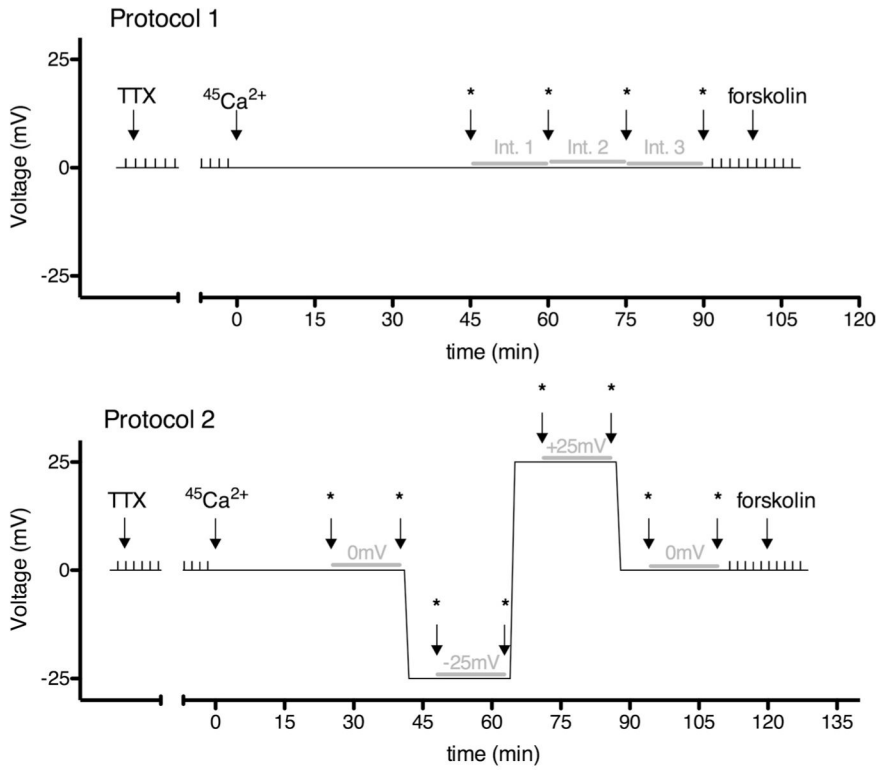

Fig. 1.

Protocols used to measure unidirectional Ca^{2+} fluxes across intestinal preparations. Either *protocol 1* (*top*) or *protocol 2* (*bottom*) were used. The transepithelial voltage across tissue preparations (*y*-axis) was clamped to the value depicted for the specific time periods (*x*-axis). Small vertical spikes correspond to 2-mV pulses applied and used to determine transepithelial resistance. In both protocols, TTX was added first (final concentration 0.1 μM) and the resistance was allowed to stabilize. Then (at a time arbitrarily set to 0), solutions were exchanged for fresh ones, with 1 side containing $^{45}Ca^{2+}$. Asterisks indicate the time points when samples were taken for radioactivity measurements. The gray horizontal lines represent the 15-min time intervals used to calculate Ca^{2+} fluxes. For *protocol 1*, 3 intervals with voltage clamped to 0 mV throughout were used. For *protocol 2*, 2 intervals with the voltage clamped to 0 mV, 1 interval with the voltage clamped to −25 mV, and 1 interval with the voltage clamped to +25 mV were used. For both protocols, forskolin (final concentration 10 μM) was added at the end of the experiment to confirm tissue viability.

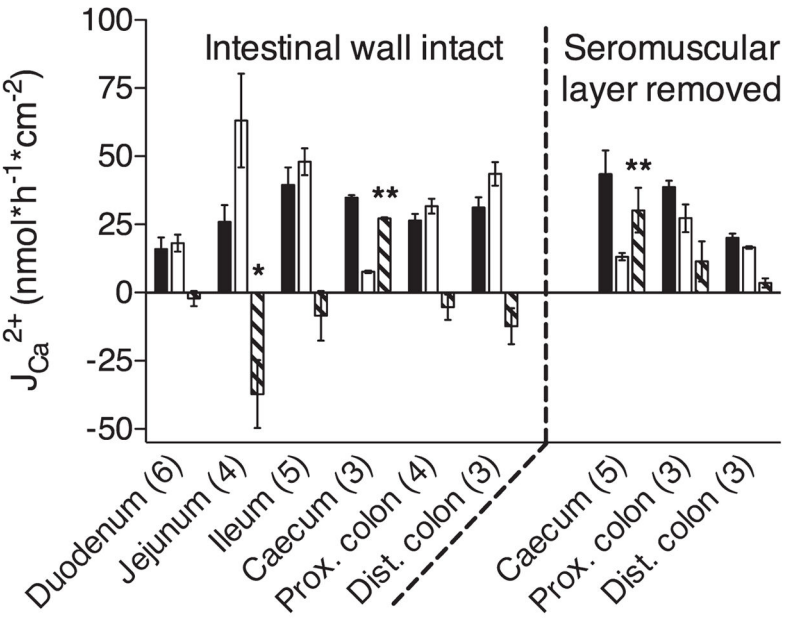

Fig. 2.

Ca^{2+} fluxes across different intestinal segments. Whole wall preparations of each intestinal segment (*left*) or sheets of epithelium with seromuscular layers stripped away (*right*) were mounted in an Ussing chamber and *protocol 1* was applied as described in MATERIALS AND METHODS. Ca^{2+} fluxes from the luminal-to-serosal (solid bars) and the serosal-to-luminal (open bars) side were measured and net fluxes (shaded bars) were calculated for each segment. Data are presented as means ± SE; numbers in parentheses indicate the number of preparations used. Asterisks indicate a net flux that is statistically different from 0 (Student's unpaired *t*-tests; $*P < 0.05$, $**P < 0.01$). Prox., proximal; Dist., distal.

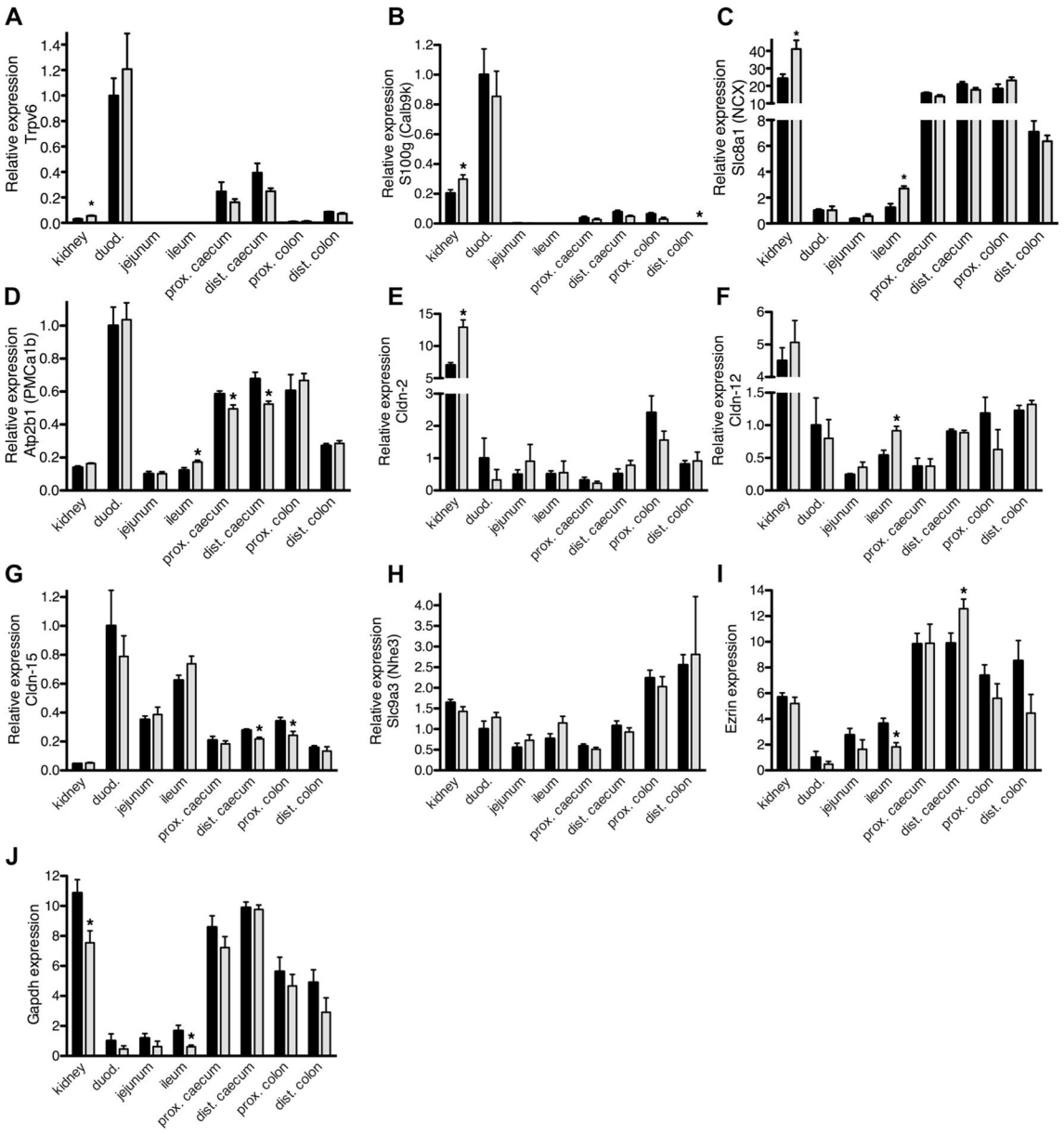

Fig. 3.

Relative mRNA expression of genes implicated in intestinal Ca^{2+} absorption. Plots of mRNA expression for kidneys and different intestinal segments, relative to the expression level in male duodenum (duod.). Data depicted in *A*–*H* are normalized to ezrin expression. All data are presented as the mean from 5 males (solid bars) or 5 females (shaded bars) ± SE. The cecum of each animal was divided in half to generate a proximal and distal part. Asterisks indicate a statistical difference between males and females (Student's unpaired *t*-tests; $*P < 0.05$). *A*: expression of Trpv6 (TRPV6). *B*: expression of S100g (Calb9k). *C*: expression of Slc8a1 (NCX). *D*: expression of Atp2b1 (PMCa1b). *E*: expression of Cldn-2. *F*: expression of Cldn-12. *G*: expression of Cldn-15. *H*: expression of Slc9a3 (Nhe3). *I*:

expression of ezrin, used for normalization of the data in *A*–*H*. *J*: expression of Gapdh. Expression of the latter 2 genes is relative to male duodenal expression.

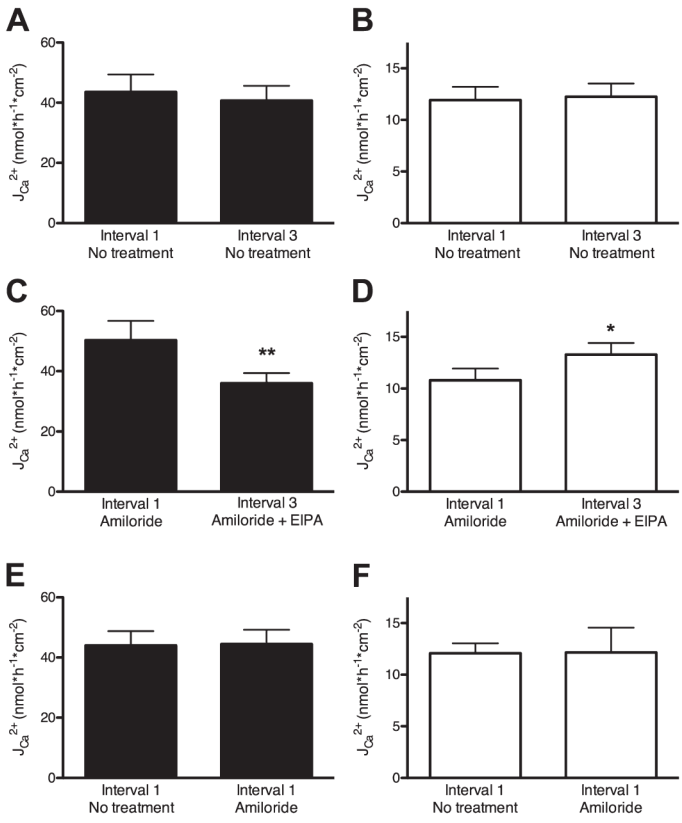

Fig. 4.

Effect of amiloride and EIPA on Ca^{2+} fluxes across mouse cecum. After stripping of the muscular layer, the cecum was mounted in an Ussing chamber. For each preparation, Ca^{2+} fluxes were measured in 3 subsequent 15-min intervals as described in MATERIALS AND METHODS (*protocol 1*, Fig. 1). Data are presented as means ± SE. Asterisks indicate a statistical difference between the flux from the first vs. the third time interval [Student's paired (*A*–*D*) and unpaired (*E* and *F*) *t*-tests; $*P < 0.05$, $**P < 0.01$]. *A* and *B*: luminal-to-serosal (*A*) and serosal-to-luminal flux (*B*) of Ca^{2+} from the first and third time interval. No additional drugs were added during these experiments, $N \geq 7$. *C* and *D*: luminal-to-serosal (*C*) and serosal-to-luminal flux (*D*) of Ca^{2+} from the first and the third intervals. Amiloride (final concentration 10 μM) was added apically before the beginning of the first interval and EIPA (final concentration 100 ± M) was added bilaterally during the second time interval, $N \geq 8$. *E* and *F*: luminal-to-serosal (*E*) and serosal-to-luminal flux (*F*) of Ca^{2+} in the first intervals of preparations pretreated with amiloride (final concentration 10 μM apically, $N \geq 14$) and without amiloride pretreatment ($N = 10$).

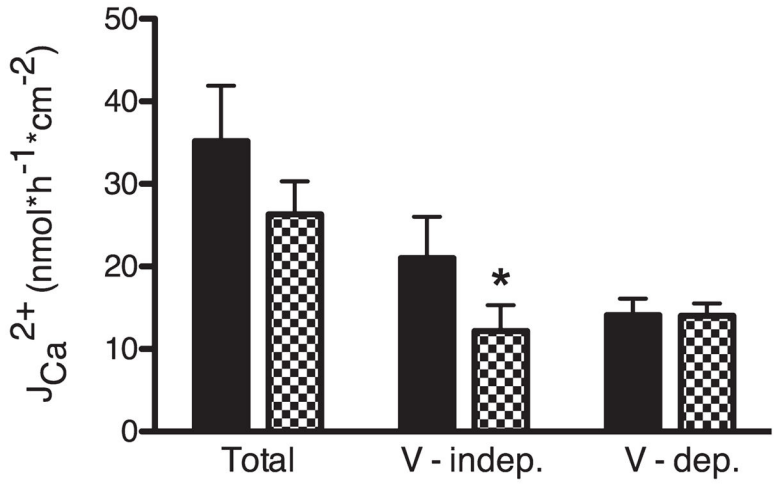

Fig. 5.

Effect of ruthenium red on luminal-to-serosal Ca^{2+} flux J_{Ca}^{2+}. Mouse cecum was stripped of the muscular layer and mounted in an Ussing chamber. Pairs of preparations from the same mouse were investigated simultaneously. One preparation was pretreated with ruthenium red (final concentration 50 μM apically, checker bars) and the other was left without additional pretreatment (solid bars). The voltage-clamp protocol as described in MATERIALS AND METHODS (*protocol 2*, Fig. 1) was applied and the luminal-to-serosal flux of Ca^{2+} measured. Total luminal-to-serosal Ca^{2+} flux as well as its voltage-dependent (V-dep.) and voltage-independent (V-indep.) components are displayed. Data presented are means ± SE. Asterisk indicates a statistical difference between the preparations pretreated with ruthenium red and their controls from the same animals (Student's paired *t*-test; $*P < 0.05$, $N = 6$).

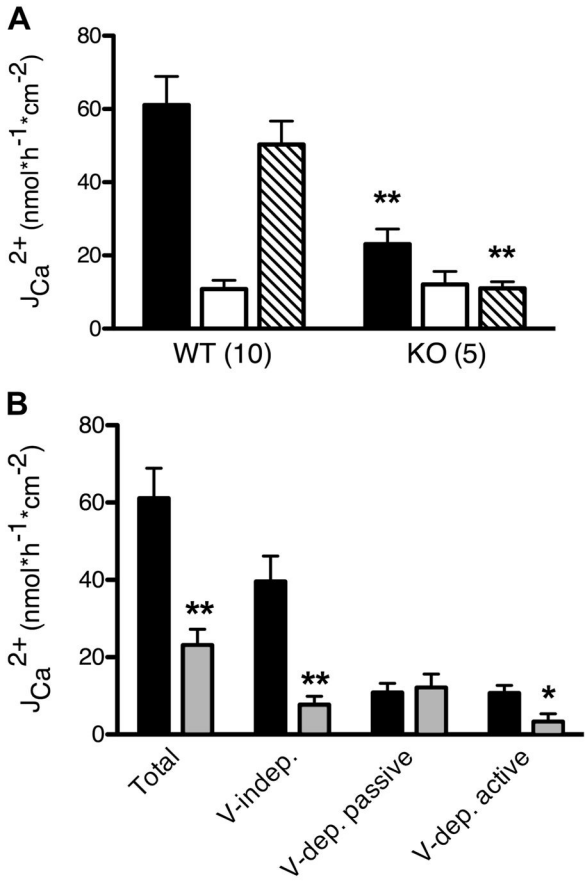

Fig. 6.

Comparison of fluxes across cecal preparations from wild-type (WT) and NHE3$^{-/-}$ (KO) mice. Mouse cecum from WT and NHE3$^{-/-}$ KO mice were stripped of the muscular layer and mounted in an Ussing chamber. The voltage-clamp protocol was applied as described in MATERIALS AND METHODS (*protocol 2*, Fig. 1). Data are presented as means ± SE. Asterisks indicate a statistical difference between values for WT vs. KO animals (Student's unpaired *t*-tests; *$P < 0.05$, **$P < 0.01$). *A*: Ca^{2+} fluxes from the luminal-to-serosal side (solid bars), from serosal-to-luminal side (open bars) and calculated net fluxes (shaded bars) in preparations from KO and WT mice. Numbers in parentheses represent number of preparations used in each experimental group. *B*: total luminal-to-serosal Ca^{2+} flux divided into voltage-independent, passive voltage-dependent, and active voltage-dependent components from WT (solid bars) and NHE3$^{-/-}$ (shaded bars) mice. Data are recounted from the experiments depicted in *A*.

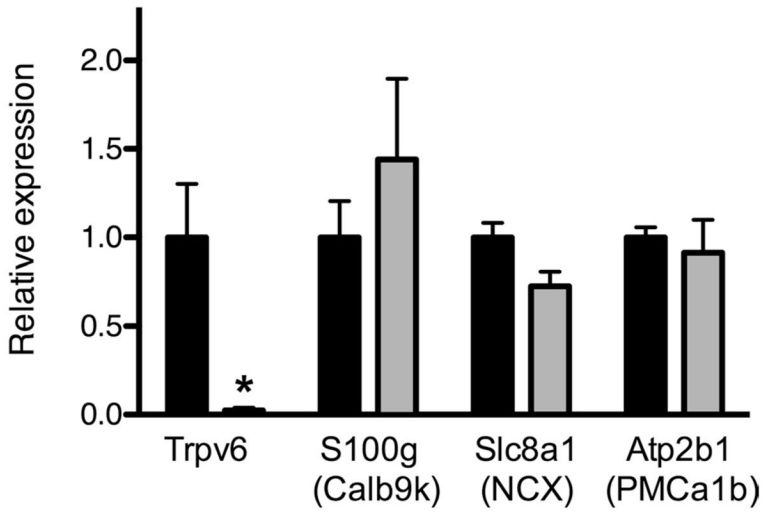

Fig. 7.

Relative cecal mRNA expression of genes implicated in transcellular Ca^{2+} flux from WT and $NHE3^{-/-}$ mice. Cecum from WT (solid bars, $N = 8$) and $NHE3^{-/-}$ KO (shaded bars, $N = 5$) mice were stripped of the muscular layer and used for quantification of mRNA expression. The expression was normalized to ezrin for each sample and relative expression is compared with WT. Data are presented as means ± SE. Asterisks indicate a statistical difference between values for WT and KO animals (Student's unpaired *t*-tests; $*P < 0.05$).

Table 1

Real-time PCR primers and probes

Calbindin-D_{9K} (S100 g)	Forward: TGGATAAGAATGGCGATGGAG
	Reverse: GCTAGAGCTTCAGGATTGGAG
	Probe: ACAGCACCTACTGATTGAACGCACG
*Nhe*3 (slc9a3)	Cat no: Mm01352473_m1 (ABI)
PMCA1b	Forward: CGCCATCTTCTGCACCATT
	Reverse: CAGCCATTGCTCTATTGAAAGTTC
	Probe: CAGCTGAAAGGCTTCCCGCCAAA
NCX (slc8a1)	Forward: TGGTCTGAAAGATTCCGTGAC
	Reverse: AGTGACATTGCCTATAGACGC
	Probe: AGCTACCCAGGACCAGTATGCAGA
Ezrin	Forward: TTCCTACCTGGCTGAAACTTG
	Reverse: TGTGATGTCCTGGATGAGTTC
	Probe: ACCCTGTCC/ZEN/AGTTTAAATTCCGGGC
Claudin-2	Forward: GCTTGTGACCCCTTGGAC
	Reverse: CTCCTTACAAGTATCTGTGGGTG
	Probe: CGTTCGCCTTTCTCTGGACCTAGT
Claudin-12	Forward: TCGCCAGAACGCACTTC
	Reverse: TGAACTCAGATGCAACAGGAG
	Probe: ATCCCGCTCACCCACTCCG
Claudin-15	Forward: CTTCCCTACAAGCCTTCTACG
	Reverse: AGACAGTGGGACAAGAAATGG
	Probe: AGCTGATGTCACTCTCATCCGAGGT

Table 2

Comparison of Ca^{2+} fluxes between proximal and distal mouse duodenum

	Proximal Portion (1.0–2.2 cm)*	Distal Portion (3.4–4.8 cm)*	*P* Value (*t*-test)
$J_{Ca^{2+}}$ Luminal-to-serosal, nmol · h^{-1} · cm^{-2}	13.6 ± 2.4	18.4 ± 1.8	0.19
$J_{Ca^{2+}}$ Serosal-to-luminal, nmol · h^{-1} · cm^{-2}	18.5 ± 2.5	17.7 ± 6.6	0.91
P value (*t*-test)	0.23	0.92	

Values of unidirectional Ca^{2+} fluxes ($J_{Ca^{2+}}$) are presented as means ± SE. Each number was calculated from 3 mice. Two segments were collected from each animal and were used to measure Ca^{2+} flux in opposite directions. The data presented here are recalculated from the numbers depicted in Fig. 2. There was no significant difference between Ca^{2+} flux in different parts of the duodenum, or between luminal-to-serosal and serosal-to-luminal flux in either the proximal or distal duodenum (Student's unpaired *t*-test, $P > 0.05$).

*Distance from pylorus.

Table 3

Properties of cecum from wild-type and NHE3$^{-/-}$ mice

	Surface Area, cm^2	Transepithelial Resistance, Ω· cm^2	Basal Short-Circuit Current, μA/cm^2
WT	7.9 ± 0.6 (12)	88.8 ± 4.7 (10)	20.8 ± 3.4 (10)
KO	19.9 ± 1.1†(6)	120.7 ± 14.3*(5)	33.9 ± 3.5*(5)

Comparison of surface area, transepithelial resistance, and basal short-circuit current for cecal preparations (after seromuscular stripping) from wild-type (WT) and NHE3$^{-/-}$ (KO) mice. Data are presented as means ± SE; numbers in brackets indicate the number of mice used in each group. The transepithelial resistance and basal short-circuit current for each animal were calculated as the average from the two paired samples. Statistically significant difference between WT and KO mice (Student's unpaired *t*-test:

$^{*}P < 0.05$;

$^{\dagger}P < 0.01$).

Table 4

Comparison of Ca^{2+} fluxes across cecum from wild-type male and female mice

		Ca^{2+} Flux, nmol · h^{-1} · cm^{-2}			Contribution to Luminal-to-Serosal Flux, %	
	Age, wk	Luminal-to-serosal	Serosal-to-luminal	Net	Voltage independent	Active voltage dependent
Males (5)	10.4 ± 0.5	64.5 ± 11.3	11.9 ± 4.5	52.7 ± 7.1	65.4 ± 2.6	17.9 ± 5.4
Females (5)	11.3 ± 1.0	57.7 ± 11.7	9.7 ± 2.0	47.9 ± 11.5	60.2 ± 5.0	21.0 ± 3.1
P value (*t*-test)	0.44	0.68	0.67	0.73	0.38	0.63

Data are presented as means ± SE; numbers in parentheses indicate the number of mice used per group. There was no significant difference in any of the investigated parameters between sexes (Student's unpaired *t*-test, $P > 0.05$).